# Epoxidation Showdown: Unveiling the Kinetics of Vegetable Oils vs Their Methyl Ester Counterparts

Yudong Meng, Elano Nery Ferreira, Nágila Maria Pontes Silva Ricardo, Nasreddine Kebir, Sébastien Leveneur

# Epoxidation showdown: unveiling the kinetics of vegetable oils vs. their methyl ester counterparts

**Yudong Meng[1,2], Elano Nery Ferreira[3], Nágila Maria Pontes Silva Ricardo[3], Nasreddine Kebir[2], Sebastien Leveneur*[,1]**

[1] INSA Rouen Normandie, Univ Rouen Normandie, Normandie Université, LSPC, UR 4704, F-76000 Rouen, France

[2] INSA Rouen Normandie, Univ Rouen Normandie, CNRS, PBS UMR 6270, F-76000 Rouen, France

[3]Laboratory of Polymers and Materials Innovation, Department of Organic and Inorganic Chemistry, Sciences Center, Federal University of Ceará, Campus of Pici, CEP 60440-900 Fortaleza, CE, Brazil

***Corresponding author:** (Sebastien Leveneur, Laboratoire de sécurité des procédés chimiques (LSPC), INSA Rouen Normandie, 685 avenue de l'Université, Saint-Étienne-du-Rouvray, France; ORCID ID: 0000-0001-9528-6440; **Email:** sebastien.leveneur@insa-rouen.fr)

## Abstract

The valorization of vegetable oils via the functionalization of their unsaturated groups has gained much interest. Epoxidation is the most common reaction for functionalizing vegetable oils into promising polymers such as non-isocyanate polyurethanes and epoxy resins. From a chemical engineering standpoint, using the esterified form of vegetable oils (VO), i.e., fatty acid methyl esters (FAMEs), is recommended to ease the mixing due to viscosity increase. To the best of the author's knowledge, no kinetic models were developed to compare the kinetics of epoxidation between vegetable oils and their corresponding FAMEs. Kinetic models were developed using different analytical methods and considering the side reaction of oligomerization for the epoxidation of linseed (LSO), cottonseed (CSO), and soybean oil (SBO) and their corresponding FAMEs using propionic acid and solid catalyst, i.e., Amberlite IR-120. The model fits quite well with the organic and aqueous phase experimental concentrations. The rate constants for epoxidation evolve in the following order: CSO>SBO>LSO. The linearity between the rate constant and initial DB concentration is more pronouced for VO-FAME than VO.

**Keywords:** structure reactivity, epoxidation, fatty acids methyl ester, kinetic modeling

# 1 Introduction

Our modern societies depend heavily on fossil materials; for example, more than 80% of chemicals and energy are produced from coal, oil or natural gas [1]. This dependency leads to several threatening situations: geopolitical tensions, economic instability, resource depletion and environmental degradation.

Biomass as raw materials in the chemical industry regained interest after the first oil crisis in 1973 [2]. The Brazilian experience with valorizing sugar cane into ethanol or food sugar illustrates the benefits of biomass in chemical industries [3]. Thus, using biomass as raw materials could overcome the difficulties linked to fossil raw materials and improve the sustainability of chemical industry.

As one type of biomass, vegetable oil is widely transformed into biodiesels [4–6] , which is mainly used in Europe as biofuel [7]. Furthermore, vegetable oils can also be valorized into polymers [8], biolubricants [9], or surfactants and Detergents [10], which attracted more researchers' interest in recent years.

Valorization of vegetable oils into fuels, materials or chemicals requires chemical transformations such as epoxidation [11], hydrogenation, transesterification, carbonation [12] and aminolysis [13]. Epoxidation of vegetable oils is one of the most essential steps for producing biobased non-isocyanate polyurethanes [14,15].

Research on this topic has continued [16] since the first studies on oil epoxidation by Wisknial et al. [17,18]. and on the preparation of vegetable epoxy resins [19,20] for various applications. There are several strategies for the production of epoxidized vegetable oils:

-Use of molecular oxygen via the oxidation of cumene [21];

-Use of hydrogen peroxide for direct epoxidation [22–25];

-Use of the Prileschajew oxidation method via the in situ production of percarboxylic acid [26–29].

The Prilschajew is the most used approach, undoubtedly because the epoxidation is faster. Nevertheless, this method leads to a liquid-liquid reaction system, where hydrogen peroxide and carboxylic acid react in the aqueous phase to produce percarboxylic acid, which diffuses into the organic phase to epoxidize the unsaturated group from the vegetable oils. Percarboxylic acid acts as an oxygen carrier because the solubility of hydrogen peroxide in the organic phase is very low, making direct epoxidation by hydrogen peroxide very challenging [30]. Fig. 1 shows the reaction steps of this system.

The drawback of this method is the mixing issue linked to the biphasic system, the risk of thermal runaway according to the nature of the carboxylic acid [31] and the side reaction of ring-opening [32,33].

The use of propionic acid instead of acetic or formic acid could decrease the risk of a thermal runaway because perpropionic acid decomposition is less exothermic than peracetic or performic acid [34]. Besides, propionic acid is a weaker acid compared to acetic or formic acid, thus the side reaction of ring-opening is less pronounced. The perhydrolysis reaction can be accelerated by the use of cation exchange resins [35].

From a chemical reactor standpoint, increased viscosity during epoxidation is a drawback because it decreases the reaction homogeneity [36]. One way to circumvent this challenge is to transesterify vegetable oil. From a previous study of our group, the epoxidation kinetic of cottonseed oil and its fatty methyl ester equivalent were compared, but the kinetic models were not developed [34]. To the best of author's knowledge, no studies are comparing the kinetics of epoxidation of vegetable oils and their fatty acid methyl ester equivalent by developing a kinetic model.

There are three approaches to develop a kinetic model for the Prileschajew system [26]: neglecting both phases and considering the whole system as homogeneous, assuming that mass transfer is very fast compared to kinetic reaction that leads to a pseudo-homogeneous approach, and taking into account the mass transfer in the material balances that leads to a biphasic approach.

This article studied the kinetics of epoxidation of three common vegetable oils and their associated FAMEs: cottonseed, soybean and linseed oils. The propionic acid was used as an oxygen carrier and Amberlite IR-120 to catalyze the perhydrolysis reaction. Several analytical methods were used to identify the different species present during this reaction, and kinetic models were developed considering the mass transfer of species between the aqueous and organic phases.

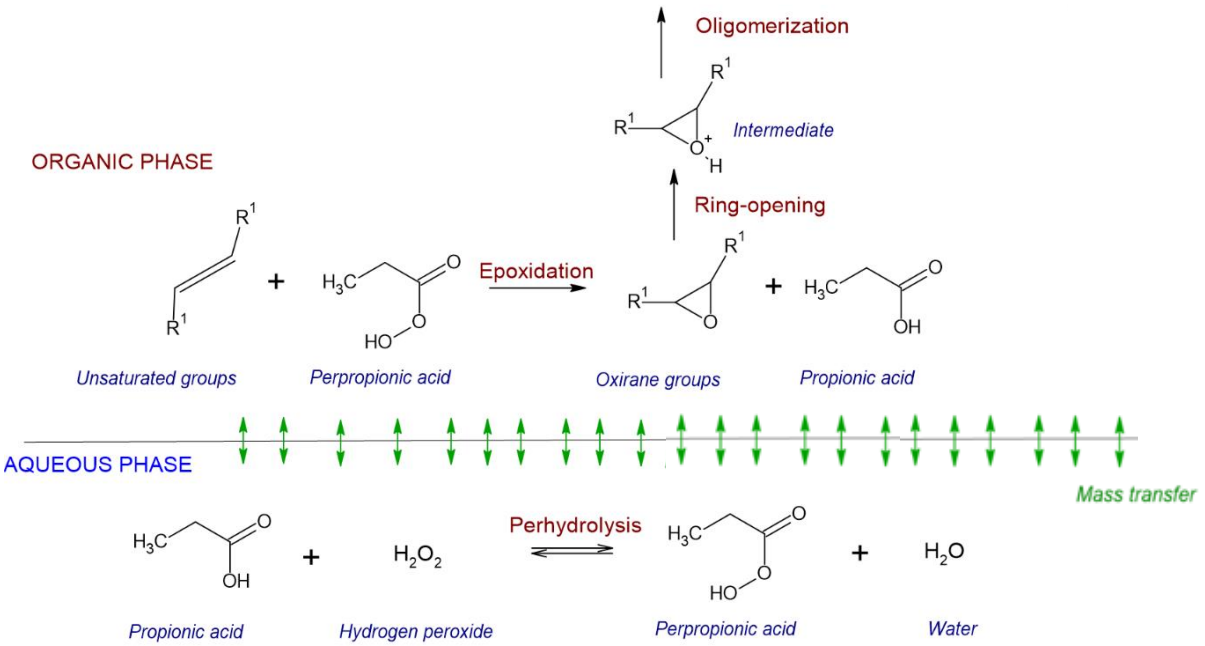


Fig. 1. Reaction steps for the epoxidation via the Prileschajew method.

# 2 Materials and Chemical

Refined cottonseed oil, soybean oil, linseed oil, propionic acid, potassium iodide and sodium thiosulfate solution (0.1 mol/L, $Na_2S_2O_3 \cdot 5H_2O$ in water) were purchased from ThermoFisher Scientific (Schwerte, Germany). Hydrogen peroxide (33 wt% in water), tetraethylammonium bromide (TEAB), dichloromethane and perchloric acid (0.1 mol/L, in acetic acid) were purchased from VWR International (Fontenay-sous-Bois, France). Magnesium sulfate, chloroform, methanol, iodine solution (0.1 mol/L, ICl in glacial acetic acid), deuterated chloroform ($CDCl_3$) and Amberlite IR-120 were obtained from Sigma-Aldrich (Burlington, USA).

## 2.1 Reactions

### 2.1.1 Esterification reaction

Esterification reactions were operated in a 400 mL glass water-jacketed reactor. Esterification of vegetable oil (VO) was performed by the mean of Campanella et al. with slight modification [37]. In brief, preheated 50 mL of methanol with 2.1g NaOH was added to 200 g warmed cottonseed oil in the reactor, and the esterification was kept at 70 °C for 1.5 h. The glycerol layer was removed after the mixture was stratified into two phases. Then, the rest of the separated methyl ester in the reactor was washed 6 times with distilled water (including 3 times with one drop of $H_3PO_4$ solution). The methyl ester was purified by an IKA RV10 control vacuum rotary evaporator (VWR, Darmstadt, Germany) with a reflux condenser at 65 °C for 1 h. The final product of CSO-FAME (SBO-FAME or LSO-FAME) was kept at 4 °C in the fridge.

### 2.1.2 Epoxidation reaction

The epoxidation reactions were carried out in a 400 mL glass-jacketed reactor with mechanical stirring, temperature probes, and a reflux condenser. In brief, a mixture of the organic phase (VOs or FAMEs), catalyst (Amberlite IR-120), and aqueous phase (33 wt% hydrogen peroxide and distilled water) were added to the reactor. Then, the preheated propionic acid was added to the reactor when the mixture was preheated to the desired temperature. The epoxidation lasted for 5 h with the rotating speed at 600 rpm. The samples were collected over time during the epoxidation. The organic and aqueous phases were analyzed and kept in a fridge at 4 °C. The effect of stirring speed on the kinetic on epoxidation was evaluated, and it was found that 600 rpm was the optimum speed. Table 1 shows the experimental matrix used to compare the kinetics and develop the kinetic model for epoxidation for each VO and each VO-FAME. Reaction temperature, catalyst loading, propionic acid, and hydrogen peroxide concentrations varied to estimate kinetic constants correctly.

Table 1 Experimental runs for the kinetics of epoxidation of Vegetable oils (CSO, SBO and LSO) and FAMEs (CSO-FAME, SBO-FAME and LSO-FAME).

| | | | Initial mass (g) | | | | Initial concentration (mol/L) | | | | |
|---|---|---|---|---|---|---|---|---|---|---|---|
| **Run** | T (K) | Catalyst | Organic[a] | 33% HP[b] | PA[c] | $H_2O$ | $[H_2O]_{aq}$ | $[DB]_{org}$ | $[Ep]_{org}$ | $[HP]_{aq}$ | $[PA]_{aq}$ |
| **1** | 343.0 | 10.0 | 100.00 | 83.00 | 74.00 | 43.00 | 27.51 | 4.02 | 0.00 | 4.03 | 4.99 |
| **2** | 333.0 | 10.0 | 100.00 | 83.00 | 74.00 | 43.00 | 27.51 | 4.02 | 0.00 | 4.03 | 4.99 |
| **3** | 323.0 | 10.0 | 100.00 | 83.00 | 74.00 | 43.00 | 27.51 | 4.02 | 0.00 | 4.03 | 4.99 |
| **4** | 333.0 | 5.0 | 100.00 | 83.00 | 74.00 | 43.00 | 27.51 | 4.02 | 0.00 | 4.03 | 4.99 |
| **5** | 333.0 | 10.0 | 100.00 | 144.50 | 44.50 | 11.00 | 29.95 | 4.02 | 0.00 | 7.01 | 3.00 |
| **6** | 333.0 | 10.0 | 100.00 | 61.80 | 103.71 | 34.35 | 21.06 | 3.85 | 0.00 | 3.00 | 7.00 |

a: organic represents all VOs and VO-FAMEs including CSO, SBO, LSO, CSO-FAME, SBO-FAME and LSO-FAME; b: HP, hydrogen peroxide; c: propionic acid.

## 2.2 Analytical methods

### 2.2.1 Density and viscosity measurement

Density was measured using a digital glass vibrating-tube densitometer (DMA5000, Anton Paar Ltd., St. Albans, U.K.) with an accuracy of $1 \times 10^{-3}$ kg·m$^{-3}$ and 0.001 K for temperature according to the manufacturer.

The dynamic and kinematic viscosity of vegetable oils and vegetable oil fatty acid methyl esters were investigated in a digital rolling-ball viscometer (Lovis 2000 ME, Anton Paar, Graz, Austria) with an accuracy of 0.5% and 0.002 °C for the temperature according to the manufacturer.

### 2.2.2 Nuclear Magnetic Resonance (NMR) analysis

$^1$H NMR analysis was investigated by using an MSL-300 NMR spectrometer (Bruker Corporation, Billerica, USA) at 300 MHz in $CDCl_3$ solutions with a TMS (tetramethylsilane) internal standard.

### 2.2.3 Fourier-Transform InfraRed spectroscopy (FTIR) analysis

FTIR analysis was investigated using Spectrum 2000 FTIR (PerkinElmer, Inc., Waltham, Massachusetts, USA) with a diamond ATR device, and the spectra were obtained from 10 scans in the range of 650 to 4000 cm$^{-1}$.

### 2.2.4 Size Exclusion Chromatography (SEC) analysis

Average molecular weights (Mn and Mw) and dispersity (Đ = Mw/Mn) were carried out by Size Exclusion Chromatography (SEC). Samples (15 mg) were dissolved in dichloromethane (2 mL) and filtered (0.45 µm). Then, the Varian PL-GPC50 system (Agilent Technologies, Santa Clara, California, USA) with two mixed packed columns (PL gel mixed type C) was applied for the analysis. The system used dichloromethane as the mobile phase and PMMA standards (from 875 to 62000 g mol$^{-1}$) for calibration.

### 2.2.5 Determination of the fatty acid compositions in vegetable oils

The fatty acid composition in vegetable oils (CSO, SBO and LSO) was determined using the NMR integrities [38]. MestReNova software was applied to integrate and analyze the peaks.

### 2.2.6 Double bond content

The concentration of double bonds in the organic phase was calculated by iodine value and measured by Wijs approach [39]. Briefly, 0.20 g sample was dissolved in 20 mL of chloroform. Then, 25 mL of Wijs solution (0.1 mol/L) was added. After one hour in the dark, 20 mL of 10% KI solution was added. Then 100 mL water was added, and the double bond concentration was titrated and calculated by $Na_2S_2O_3$ solution (0.1 mol/L) with an auto-titrator (916 Ti-Touch, Methrohm, Herisau, Switzerland). The normalized concentration of double bond is calculated by: $[DB]_n = \frac{[DB]}{[DB]_0}$, where $[DB]_n$ is the normalized concentration of double bond, $[DB]_0$ is the concentration of the initial concentration of double bond.

### 2.2.7 Epoxide content

Maerker's approach was applied to measure the concentration of the epoxide group in the organic phase [40]. Briefly, 100 mg sample was dissolved in 10 mL of chloroform. Then, 10 mL of TEAB solution (20% TEAB in acetic acid) was added. The concentration of the epoxidized group was titrated and calculated by perchloric acid in acetic acid solution (0.1 mol/L) with an auto-titrator. The normalized concentration of epoxide group is calculated by: $[EP]_n = \frac{[EP]}{[DB]_0}$, where $[EP]_n$ is the normalized concentration of epoxide group.

### 2.2.8 Hydrogen peroxide content

The concentration of hydrogen peroxide in the aqueous phase was determined by Greenspan and MacKellah's method [41]. Briefly, 0.10 g sample was dissolved in 50 mL of 10% sulfuric acid (in water). Three drops of Ferroin indicator were added. Then, ammonium cerium sulfate solution (0.1 mol/L) was used as the titrate solution, and light blue is the endpoint.

### 2.2.9 Concentration of acid

The concentration of acid in the aqueous phase was measured by acid-base titration method [42]. For that, 0.15 g sample was dissolved in 50 mL distilled water and titrated by sodium hydroxide solution (0.1 mol/L) with an auto-titrator.

# 3 Results and discussion

## 3.1 Characterization analysis

Density and viscosity measurements were employed to compare the fundamental physicochemical properties of different VOs and FAMEs across various temperatures. Additionally, spectroscopic techniques, including FTIR, NMR, and SEC, were utilized further to characterize the VOs and FAMEs after the epoxidation reaction. These techniques facilitated a deeper understanding of side reactions, such as ring-opening and oligomerization reactions.

### 3.1.1 Density analysis

Fig. 2. presents the linear relationship of densities of linseed oil, soybean oil, cottonseed oil, and their corresponding fatty acid methyl esters (FAMEs). All values standard errors are lower than 0.01 g/cm$^3$ (Table S1). Following esterification, there was a noticeable decrease in the densities of FAMEs, ranging from 5% to 6%. Both the densities of VOs and FAMEs decrease with the increasing temperature. The densities of VOs vary depending on their specific fatty acid compositions [43]. Table S1 indicates that LSO has the highest density, whereas SBO and CSO have similar densities due to their predominantly oleic and linoleic acid compositions. The density of linolenic acid is higher than that of linoleic acid and oleic acid. Hence linseed oil has a higher density [44].

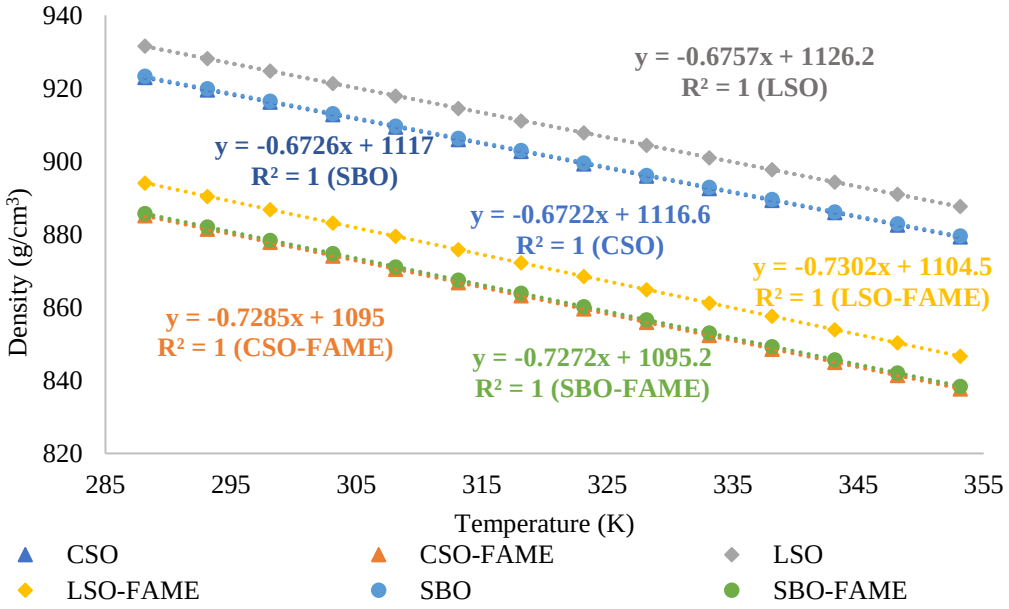


Fig. 2. Densities of CSO, SBO and LSO; and their corresponding FAMEs.

### 3.1.2 Viscosity analysis

Fig. 3 shows the linear dependence for the logarithm of dynamic viscosity and kinematic viscosity on the temperature, where a linear decrease in viscosity is visible. Tables S2 and S3 exhibit the dynamic and kinematic viscosities values with standard errors, respectively. As expected, the dynamic and kinematic viscosities of CSO, LSO, SBO, and their FAMEs decrease logically with increasing temperature. The viscosity of fatty acid methyl esters is significantly lower than that of vegetable oil, indicating that esterification can significantly reduce the viscosities, improving their fluidity and flowability. Indeed, esterification reduces the molecular weight and entanglement of hydrocarbon chains, reducing viscosity.

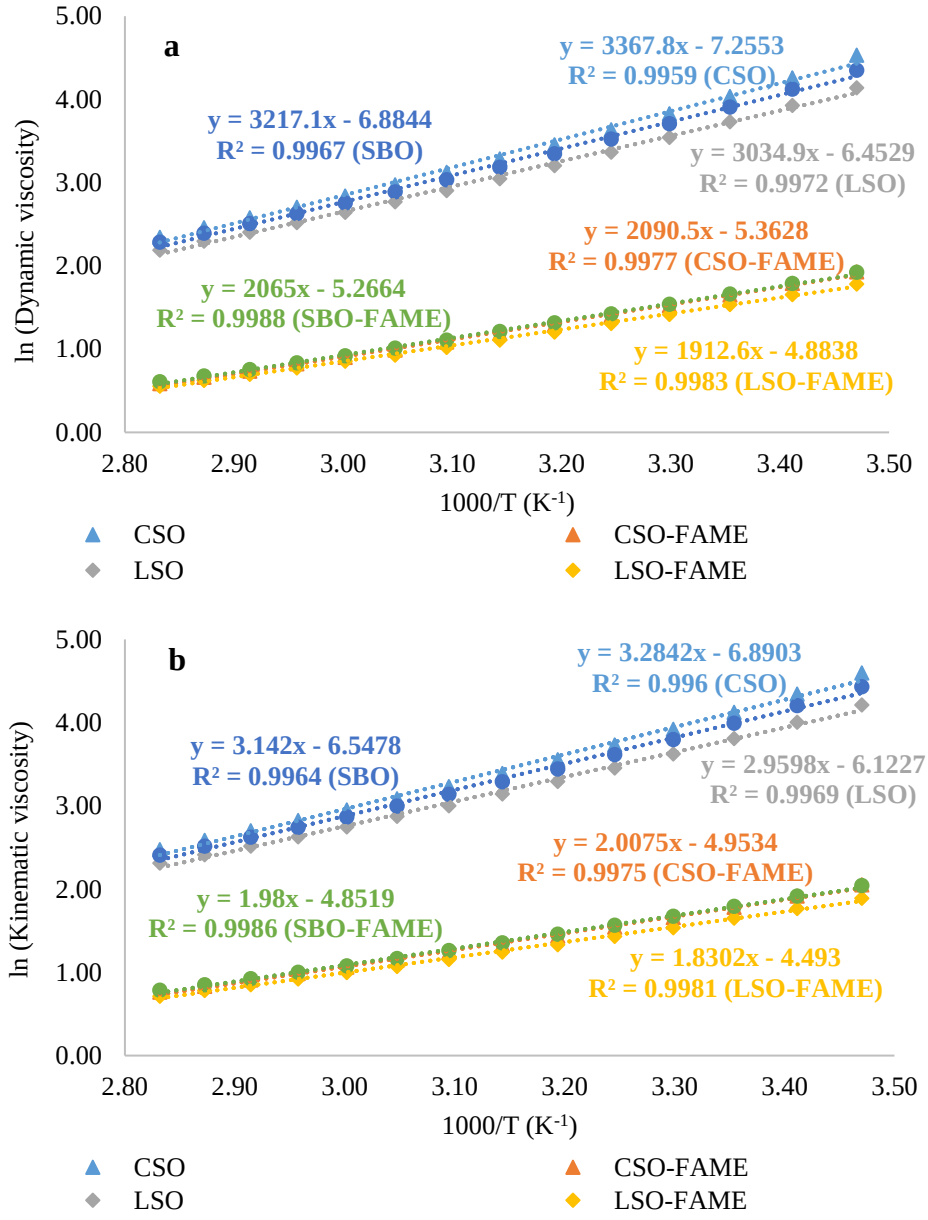


Fig. 3. Dependence of natural logarithm of dynamic viscosity (a) and kinematic viscosity (b) on inverse temperature 1000/T ($K^{-1}$) of CSO, SBO, and LSO; and their corresponding FAMEs.

### 3.1.3 FTIR analysis

Fig. 4. (and Figs S1-S2) compared FTIR spectra of VOs (CSO, SBO and LSO), VO-FAME, epoxidized VOs, and epoxidized VO-FAMEs. In accordance with our previous study, peaks above 1500 $cm^{-1}$ are consistent between FAME and VO [34]. The persistence of the band around 3000 $cm^{-1}$ (stretching vibration of H-C=) signifies stable carbon-carbon double bonds post-esterification, observed in VO-FAMEs. The 900–1500 $cm^{-1}$ range discriminates between VO and VO-FAME, with a notable band at approximately 1450 $cm^{-1}$ attributed to the asymmetric stretching vibration of C-H in methyl ester groups. The band around 1200 $cm^{-1}$ corresponds to O–$CH_3$ stretching in methyl ester groups. From 1700 to 1800 $cm^{-1}$, bands correspond to C=O stretching, indicative of esters present in both VO and VO-FAME [45]. After the epoxidation reaction, the transformation of the double bond (CH=CH) into oxirane is indicated by the disappearance of the band around 3000–3050 $cm^{-1}$ and the appearance of a band representing the epoxidized group at approximately 850 $cm^{-1}$ [46]. However, the residual band at around 3000 $cm^{-1}$, which could be found in the spectrum of ELSO and ELSO-FAME, indicates that some double bonds remained after epoxidation.

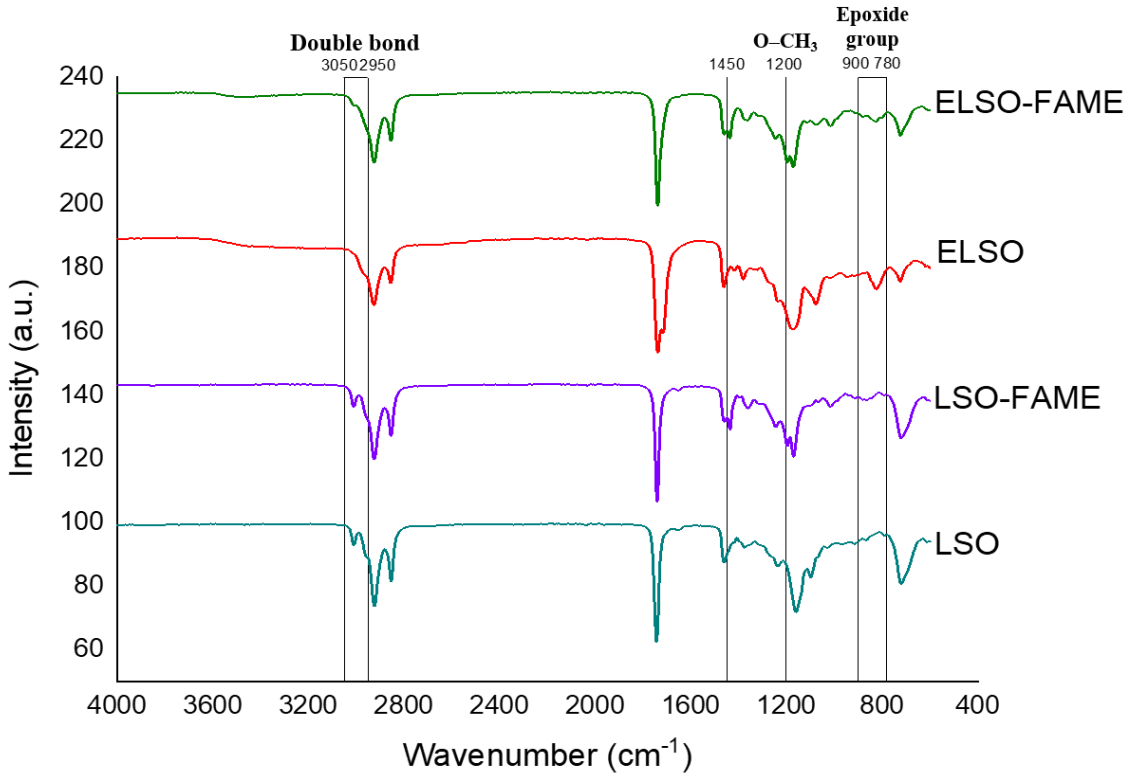


Fig. 4. FTIR spectra for the LSO, LSO-FAME, ELSO and ELSO-FAME.

### 3.1.4 NMR analysis

The NMR spectra displayed in Fig. 5 (and Figs S3-S4) illustrate the chemical structure variations between VOs (VO), VO-FAME, epoxidized VOs (EVO), and epoxidized VO-FAME (EVO-FAME). In the VO-FAME spectrum, the presence of the methyl ester group (a singlet signal at 3.7 ppm) is evident, replacing the signal attributed to $CH_2$ groups in the glyceridic part, existing before the trans-esterification, which typically resonates at 4.2 ppm. Additionally, a decrease in integration of the sharp peak around 5.2 ppm is observed due to the disappearance of the CH proton peak in the glyceridic part, which overlaps with the olefinic protons peak [47].

Following the epoxidation of VO and VO-FAME, the disappearance of the double bond peak (around 5.2 ppm) is evident, replaced by an epoxidized group peak (around 3.0 ppm). Compared with SBO and CSO, not all peaks around 5.2 ppm disappeared in LSO spectrum, meaning some double bonds left after the reaction due to the higher concentration of double bonds, which is consistent with FTIR analysis. The methyl ester group is also observable in the EVO-FAME spectrum, along with the absence of the four glyceridic proton signals at 4.2 ppm [48]. The absence of signals between 3.6 and 3.8 ppm in the $^1H$ NMR spectra indicates the non-appearance of hydroxyl groups, stemming from either the hydrolytic degradation of triglycerides in EVO or hydrolytic epoxide ring opening in both EVO and EVO-FAME, as evidenced by the integrations of proton peaks at the alpha position to the oxygen of the ester groups.

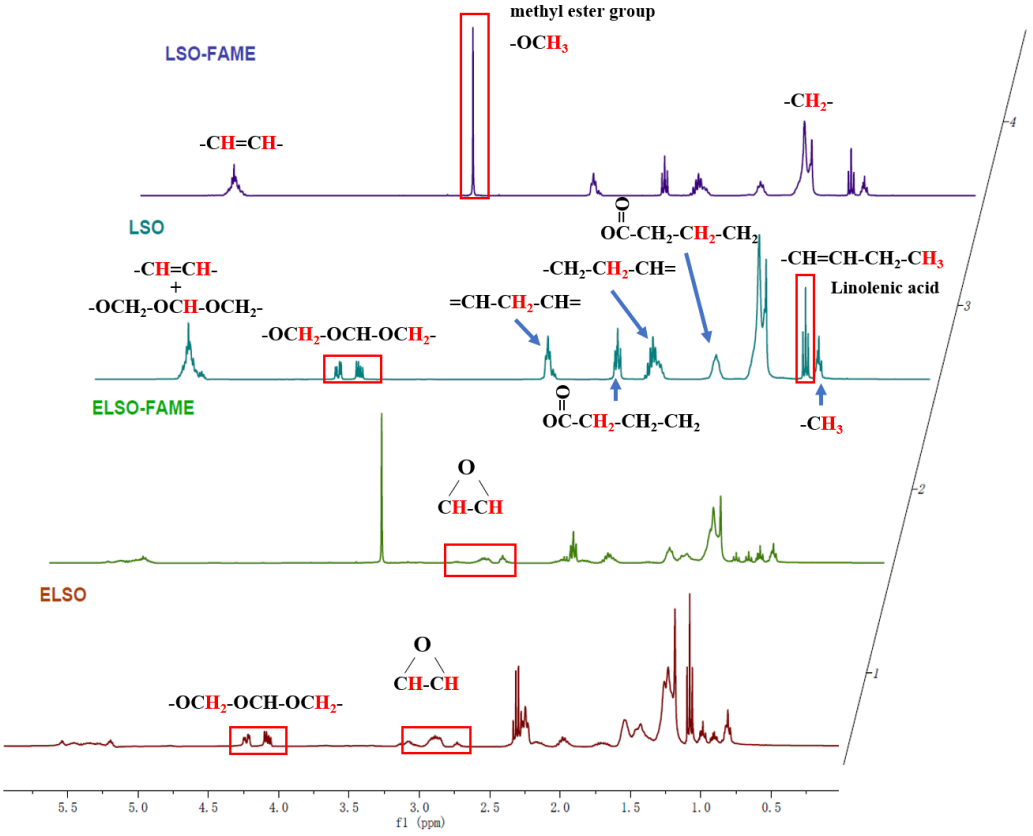


Fig. 5. $^{1}$H NMR spectra for LSO, LSO-FAME, ELSO and ELSO-FAME.

### 3.1.5 SEC analysis

As displayed in Fig. 6 (and Figs S5-S6), SEC results show a narrow main peak in VOs corresponding to the triglyceride molecules. A lower average molecular weight could be observed after the esterification because of the decomposition of the triglyceride molecules into three smaller fatty methy-ester molecules, after total glycerol removing. A shift of the main peak to the left after the epoxidation indicates the higher molecular weight due to the production of the oxirane rings. A secondary peak that can also be observed in both EVOs and EVO-FAMEs is ascribed to oligomers resulting from ring-opening/cationic polymerization reactions [49]. By comparing with ECSO, these secondary peaks exhibited higher intensity values (concentrations) in the case of ESBO and ELSO, indicating that more polymerization occurred due to the ring-opening, which could be related to a higher concentration of epoxide groups, associated with a higher initial concentration of carbon-carbon double bonds, in these two EVOs. On the other hand, no significant difference was observed between EVO-FAMEs, which displayed weak polymerization extent. It is noteworthy that for the same polymerization degree, the increase in the molecular weight of VOs is higher than corresponding EVO-FAMEs since the repeating unit of EVOs is at least 3 times higher than that of their corresponding EVO-FAMEs.

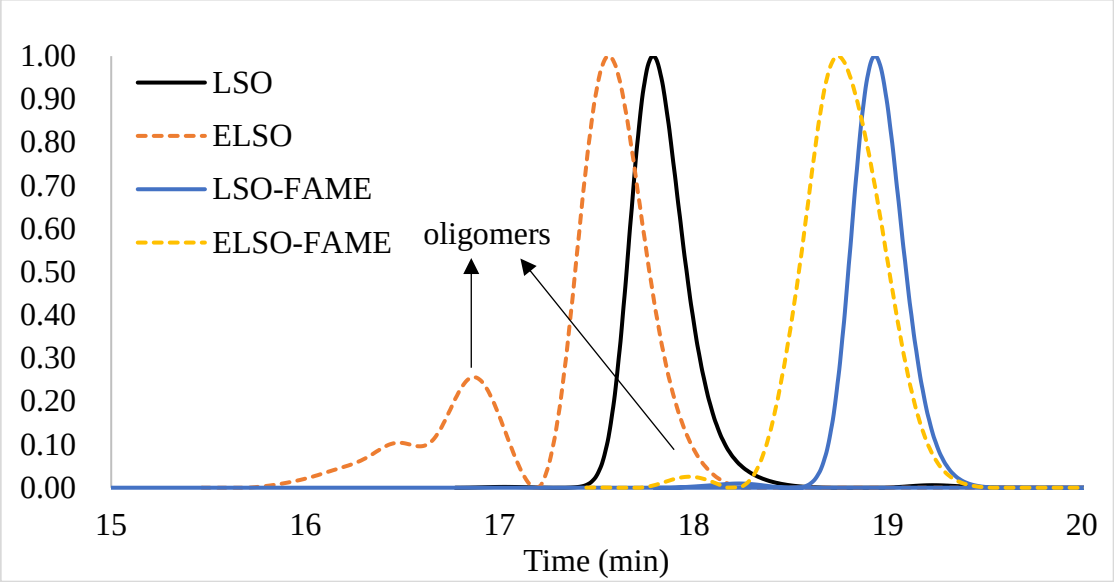


Fig. 6. SEC results for LSO, LSO-FAME, ELSO and ELSO-FAME.

### 3.1.6 Fatty acid composition

Table 2 shows the fatty acid composition of CSO, SBO, and LSO. Linolenic acid has three double bonds, linoleic has two double bonds, and oleic has only one double bond. LSO has the highest concentration of double bonds (5.79 mol/L) due to the largest amount of linolenic acid (50%). Instead of finding linolenic acid, linoleic acid is the main resource for the double bond in CSO (>50%). For SBO, linoleic acid is the majority unsaturated fatty acid, and also with some linolenic acid.

Table 2 Fatty acid composition of Vegetable oils (CSO, SBO and LSO)

| | Linolenic acid | Linoleic acid | Oleic acid | MUFA | PUFA | $TOT_s$ | $[DB]_0$ (mol/L) |
|---|---|---|---|---|---|---|---|
| **CSO** | - | 53.53% | 19.21% | 19.21% | 53.53% | 27.26% | 3.65 |
| **SBO** | 8.75% | 49.05% | 25.39% | 25.39% | 57.80% | 16.81% | 4.35 |
| **LSO** | 49.72% | 14.18% | 26.02% | 26.02% | 63.90% | 10.08% | 5.79 |

$TOT_s$: total saturated fatty acids; MUFA: mono-unsaturated fatty acid; PUFA: polyunsaturated fatty acids

## 3.2 Kinetic comparison for Epoxidation of Vegetable Oils and its FAMEs

### 3.2.1 Kinetics for epoxidation of vegetable oils

Fig. 7 shows the kinetics of double bond consumption and epoxide production for different vegetable oils, via the use of normalized concentration. The measurement was triplicated, and the standard deviation for DB and Ep was lower than 0.03 mol/L for experiments with VO. Table S4 shows the conversion and selectivity after 300 min reaction for all runs. One can observe the presence of side reactions because the final normalized concentration is different from 1 for the epoxidized concentration. Kinetics of double bond consumption evolve in the following order CSO>SBO>LSO, which is the same for the kinetics of epoxide formation. The kinetics of epoxidation vary when vegetable oils contain different fatty acid compositions and double bond concentrations. As shown in Fig. 7, the kinetic comparison with three different vegetable oils in Run 5, with the initial condition of 7 mol/L of HP and 3 mol/L of PA. Run 5 provides a higher HP concentration, which leads to a higher conversion and faster epoxidation rate. It can be observed that CSO had a faster production rate of the oxirane ring than SBO and LSO. This can be explained by the lower double bond accessibility from linolenic acid moiety slowing down the kinetics of epoxidation. Linolenic acid contains more double bonds than linoleic and oleic acids, especially with the first double bond located at the third carbon (from the methyl group), making it more accessible for ring-opening reactions. Furthermore, more oligomers were found in LSO due to the ring opening of the oxirane ring located at the third carbon, and then the epoxidation could be difficult to reach the double bonds at sixth and ninth carbon (lower conversion of [DB] in LSO). This observation of more side reactions in LSO and SBO is also consistent with the spectral analysis above.

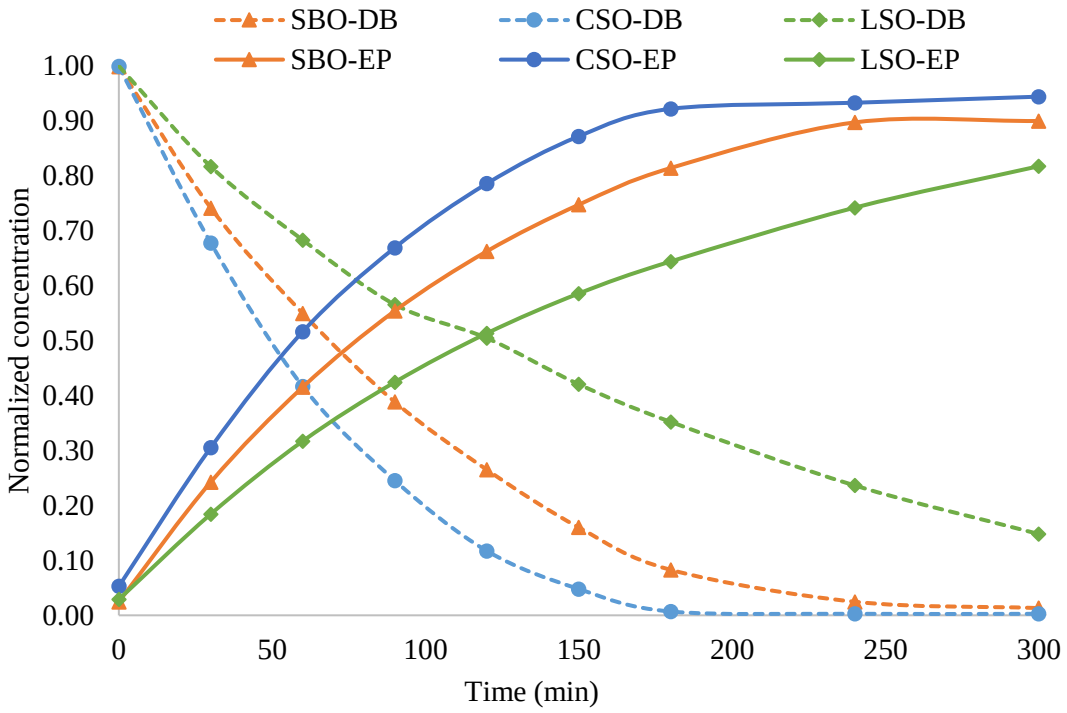


Fig. 7. Kinetic comparison between vegetable oils of RUN5 with the initial condition of 7 mol/L of HP and 3 mol/L of PA at 330.53 K.

### 3.2.2 Kinetics for Epoxidation of Vegetable Oils Fatty Acid Methyl Esters

The kinetics comparison for epoxidation of VO-FAMEs of Run 5 is displayed in Fig. 8. The measurement was triplicated, and the standard deviation for DB and Ep was lower than 0.02 mol/L for experiments with VO-FAME. Consistent with our previous studies, VO-FAMEs present higher side reactions than VOs under the same conditions. Furthermore, it could be noticed that VO-FAMEs (< 80%) have a lower selectivity than VOs (> 90%) in Table S4. The epoxidized CSO-FAME and SBO-FAME show similar behaviors on the conversion of epoxidation and the consumption rate for double bonds. As for LSO-FAME, it could be evident to observe the lower kinetic rate on the epoxidation and more ring-opening even with a higher HP concentration in Run 5. The different fatty acids methyl esters could also explain this lower kinetic rate, LSO-FAME is mainly of methyl linolenate which is the unsaturated FAME with 3 double bonds. With a higher reactivity of more double bonds in LSO-FAME, the ring opening also occurs more during epoxidation. Lower conversion could be found in LSO-FAME as well even with a lower polymerization of ring-opening products.

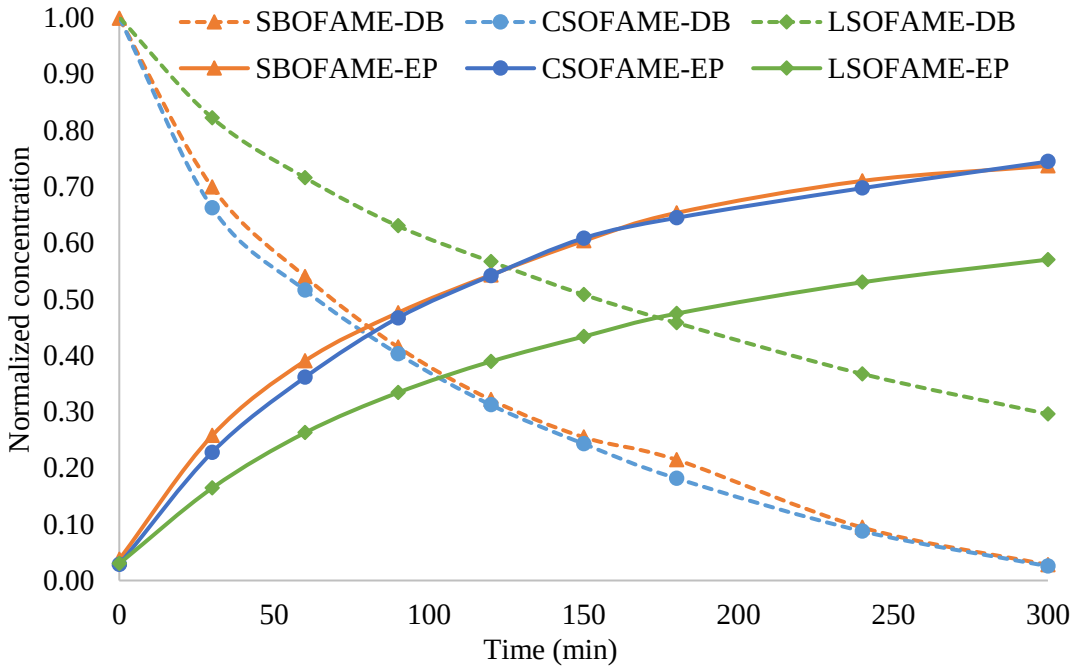


Fig. 8. Kinetic comparison between vegetable oil FAMEs of Run 5 with the initial condition of 7 mol/L of HP and 3 mol/L of PA at 333 K.

## 3.3 Kinetic modeling

### 3.3.1 Kinetics

Based on the previous studies [50], three main reactions are involved in the epoxidation of VOs and VO-FAMEs: perhydrolysis of propionic acid, epoxidation of the double bond (-CH=CH-) by perpropionic acid, and oxirane ring-opening side reaction.

The perhydrolysis expression rate was expressed as:

$$R_{Perh} = k_{Perh} \cdot m_{dried\ cat} \cdot \left( [PA]_{aq} \cdot [HP]_{aq} - \frac{1}{K_{eq}} \cdot [PPA]_{aq} \cdot [W]_{aq} \right) \quad (1)$$

where, $K_{eq}$ is the equilibrium constant and $m_{dried\ cat}$ is the dried Amberlite IR-120 after washing by water.

The expression rate for the epoxidation was expressed as:

$$R_{Ep} = \frac{k_{Ep} \cdot [PPA]_{org} \cdot [DB]_{org}}{1 + Coef_1 \cdot [RO]_{org}} \quad (2)$$

where, $[DB]_{org}$ is the concentration of the unsaturated group from the organic phase. $Coef_1$ (Coefficient 1) is a coefficient representing the hindrance linked to ring-opening reaction slowing down epoxidation reaction.

Following our previous study [51], the ring-opening reaction was derived by assuming that the rate-determining step is the protonation of the oxirane group. The expression rate for the ring-opening was expressed as:

$$R_{RO} = k_{RO} \cdot [Ep]_{org} \cdot \left( [PA]_{aq} \cdot [W]_{aq} \right)^{0.5} \quad (3)$$

In equation (3), the protons were obtained from the dissociation of propionic acid in the aqueous phase. The proton transfer from the aqueous to the organic phase is supposed to be very fast. Protons from the Amberlite IR-120 are mainly located inside the resins making their access for oxirane difficult, thus, ring-opening by Amberlite IR-120 was neglected [26,51,52].

### 3.3.2 Material balances

Due to vigorous stirring, no macroscopic gradient was considered. Kinetic experiments were performed in isothermal mode. The solubilities of the organic phase and its derivatives in the aqueous

phase, as well as hydrogen peroxide and water in the organic phase, were neglected. The aqueous phase was continuous, and it was assumed that this phase primarily wetted the catalyst. The volumes of both phases were assumed to be constant throughout the reaction.

The double-film theory was applied to account for mass transfer, assuming negligible resistance from the continuous aqueous phase. Thus, the concentration of species $i$ at the aqueous interface, denoted as $[i]^*_{aq}$, was equivalent to the concentration in the bulk aqueous phase, denoted as $[i]_{aq}$.

$$K_i = \frac{[i]^*_{aq}}{[i]^*_{org}} \tag{4}$$

where, $[i]^*_{org}$ is the concentration of compound i at the organic interface. The concentration $[i]^*_{org}$ can be expressed as: $[i]^*_{org} = \frac{[i]^*_{aq}}{K_i} \approx \frac{[i]_{aq}}{K_i}$.

Material balances for the different species are:

$$\frac{d[DB]_{org}}{dt} = -R_{Ep} \tag{5}$$

$$\frac{d[Ep]_{org}}{dt} = R_{Ep} - R_{RO} \tag{6}$$

$$\frac{d[RO\ products]_{org}}{dt} = R_{RO} \tag{7}$$

$$\begin{aligned} \frac{d[PA]_{org}}{dt} &= R_{Ep} + \frac{k_{PA-org} \cdot a \cdot V_{liq}}{V_{org}} \cdot \left([PA]^*_{org} - [PA]_{org}\right) \\ &= R_{Ep} + \frac{k_{PA} \cdot a \cdot V_{liq}}{V_{org}} \cdot \left(\frac{[PA]_{aq}}{K_{PA}} - [PA]_{org}\right) \end{aligned} \tag{8}$$

$$\begin{aligned} \frac{d[PPA]_{org}}{dt} &= -R_{Ep} + \frac{k_{PPA-org} \cdot a \cdot V_{liq}}{V_{org}} \cdot \left([PPA]^*_{org} - [PPA]_{org}\right) \\ &= -R_{Ep} + \frac{k_{PPA-org} \cdot a \cdot V_{liq}}{V_{org}} \cdot \left(\frac{[PPA]_{aq}}{K_{PPA}} - [PPA]_{org}\right) \end{aligned} \tag{9}$$

$$\begin{aligned} \frac{d[PA]_{aq}}{dt} &= -R_{Perh} - \frac{k_{PA-org} \cdot a \cdot V_{liq}}{V_{aq}} \cdot \left([PA]^*_{org} - [PA]_{org}\right) \\ &= -R_{Perh} - \frac{k_{PA-org} \cdot a \cdot V_{liq}}{V_{aq}} \cdot \left(\frac{[PA]_{aq}}{K_{PA}} - [PA]_{org}\right) \end{aligned} \tag{10}$$

$$\frac{d[PPA]_{aq}}{dt} = R_{Perh} - \frac{k_{PPA-org} \cdot a \cdot V_{liq}}{V_{aq}} \cdot \left([PPA]^{*}_{org} - [PPA]_{org}\right) = R_{Perh} - \frac{k_{PPA-org} \cdot a \cdot V_{liq}}{V_{aq}} \cdot \left(\frac{[PPA]_{aq}}{K_{PPA}} - [PPA]_{org}\right) \quad (11)$$

$$\frac{d[HP]_{aq}}{dt} = -R_{Perh} \quad (12)$$

$$\frac{d[W]_{aq}}{dt} = R_{Perh} \quad (13)$$

where, $k_{PPA-org}$ and $k_{PA-org}$ are mass transfer coefficients of PA and PPA in the organic phase. The interfacial area between the organic and aqueous phases is denoted as $a$. The distribution coefficients for PA and PPA are $K_{PA}$ and $K_{PPA}$. In Equations (5)-(13), bulk concentrations in both the aqueous and organic phases were used. $K_{PA}$ and $K_{PPA}$ for each model were calculated by the experiment data at the end of the reaction: $K_{PA} = \frac{[PA]_{aq}}{[PA]_{org}}$, and $K_{PPA} = \frac{[PPA]_{aq}}{[PPA]_{org}}$ (Table 3).

Table 3. $K_{PA}$ and $K_{PPA}$ values in different model

| | **CSO** | **CSO-FAME** | **SBO** | **SBO-FAME** | **LSO** | **LSO-FAME** |
|---|---|---|---|---|---|---|
| **$K_{PA}$** | 1.72 | 1.03 | 1.80 | 1.30 | 1.58 | 1.28 |
| **$K_{PPA}$** | 1.20 | 0.40 | 0.10 | 0.18 | 0.17 | 0.19 |

### 3.3.3 Regression

Regression was performed using Athena Visual Studio Plus V20.0 based on the Bayesian framework. Ordinary differential equations from the material balances were solved by the DDAPLUS solver, which employs a modified Newton algorithm [53,54]. The non-linear subroutine executed the GREGPLUS regression, which minimizes the objective function (OF), determines credible intervals for each estimated parameter using the marginal highest posterior density (HPD), and calculates the normalized parameter covariance. The GREGPLUS subroutine minimizes the OF via successive quadratic programming. GREGPLUS subroutine minimizes the objective function via successive quadratic programming [55].

The objective function is:

$$OF = (a + b + 1) \cdot ln|\upsilon| \quad (14)$$

where, $|\upsilon|$ is the determinant of the covariance matrix of the responses, b is the number of responses and a is the number of events in response.

Each element of this matrix is:

$$v_{ij} = \sum_{u=1}^{n} \left[C_{iu} - \hat{C}_{iu}\right] \cdot \left[C_{ju} - \hat{C}_{ju}\right] \quad (15)$$

with $C_{iu}$ the experimental concentration and $\hat{C}_{iu}$ the estimated value for response $i$ and event $u$; $C_{ju}$ the experimental concentration and $\hat{C}_{ju}$ the estimated value for response $j$ and event $u$.

Several observables can be used for epoxidation. Van Boekel suggested that the Bayesian framework is more suitable than the non-linear least squares approach for such multiresponse system [56].

It is vital to use a modified Arrhenius equation to express the temperature-dependency of the rate constants [57]

$$k_{rx}(T) = exp\left[ln\left(k_{rx}(T_{ref})\right) + \frac{E_{a_{rx}}}{R \cdot T_{ref}} \cdot \left(1 - \frac{T_{ref}}{T}\right)\right] \quad (16)$$

where, $k_{rx}(T)$ is the rate constant for reaction $rx$ at reaction temperature $T$, $E_{a_{rx}}$ is the activation energy of reaction $rx$, $R$ is the ideal gas constant, and $T_{ref}$ is the reference temperature.

### 3.3.4 Kinetic model of epoxidation of VOs and FAMEs

We used the kinetic constants from previous work for the perhydrolysis of propionic acid [50]. In the prehydrolysis model, $K_{Perh}(T_{ref} = 303.15K)$ was found to be 2.051 and $\Delta H_{Perh}$ to -4.17 kJ/mol. The kinetic constants $ln\left(k_{Perh}(T_{ref} = 343.15K)\right)$ was estimated to be -8.571 L/mol/g of dried cat/min and $\frac{E_{a_{Perh}}}{R \cdot T_{ref}}$ was found to be 16.871.

The Prileschajew method for the epoxidation of vegetable oils requires the estimation of several parameters [58]. A kinetic model for perhydrolysis using propionic acid, water, hydrogen peroxide, and Amberlite IR-120 has already been developed [50].

For the models of CSO, SBO, LSO, CSO-FAME, SBO-FAME and LSO-FAME, six observables ($[Ep]_{org}$, $[DB]_{org}$, $[PA]_{aq}$, $[PPA]_{aq}$ and $[HP]_{aq}$,) were used to estimate kinetic constants and mass transfer parameters. The ratio of the mass in organic and aqueous phases was kept constant.

ODEs were solved and the following parameters were estimated: $ln\left(k_{Ep}(T_{ref})\right)$, $\frac{E_{a_{Ep}}}{R \cdot T_{ref}}$, $ln\left(k_{RO}(T_{ref})\right)$, $\frac{E_{a_{RO}}}{R \cdot T_{ref}}$, $ka_{PA\_org}$ , $Coef_1$. Table 4 shows the estimated values with their credible intervals. Most of the HPD, except $\boldsymbol{Coef_1}$, is lower than 20% the degree of certainty is high. As a coefficient of $[RO]$ which used in $R_{Ep}$, $\boldsymbol{Coef_1}$ has less impact on the reaction rate of epoxidation.

A lower rate constant of ring opening was found in the system of propionic acid with amberlite compared to the previous study on the epoxidation of formic acid ($k_{ROPFA}$=0.0592 $L/mol/s$ at 340K) [26].

Table 4. Estimated parameters and their credible intervals for the epoxidation of CSO, SBO, LSO, CSO-FAME, SBO-FAME and LSO-FAME at $T_{ref}$= 343.15 K.

| Parameters | Unit | Origin[a] | Estimate | HPD | HPD_% |
|---|---|---|---|---|---|
| $\ln k_{Ep}(T_{ref})$[b] | - | LSO | -2.93 | 0.27 | 9.12 |
| | | SBO | -2.28 | 0.43 | 18.68 |
| | | CSO | -0.66 | 0.35 | 52.19 |
| | | LSO-FAME | -3.44 | 0.96 | 28.05 |
| | | SBO-FAME | -2.17 | 0.27 | 12.45 |
| | | CSO-FAME | -1.52 | 0.56 | 36.90 |
| $\frac{E_{a,ep}}{R_g \cdot T_{ref}}$ | - | LSO | 18.36 | 3.02 | 16.45 |
| | | SBO | 13.28 | 4.50 | 33.91 |
| | | CSO | 21.73 | 2.42 | 11.12 |
| | | LSO-FAME | 26.96 | 5.45 | 20.23 |
| | | SBO-FAME | 28.37 | 3.61 | 12.72 |
| | | CSO-FAME | 30.51 | 3.70 | 12.13 |
| $\ln k_{RO}(T_{ref})$[b] | - | LSO | -8.03 | 0.14 | 1.72 |
| | | SBO | -8.60 | 0.13 | 1.57 |
| | | CSO | -8.46 | 0.08 | 0.96 |
| | | LSO-FAME | -7.49 | 0.13 | 1.73 |
| | | SBO-FAME | -7.64 | 0.12 | 1.53 |
| | | CSO-FAME | -7.76 | 0.06 | 0.82 |
| $\frac{E_{a,Ro}}{R_g \cdot T_{ref}}$ | - | LSO | 15.44 | 4.27 | 27.64 |
| | | SBO | 4.35 | 4.11 | 94.48 |
| | | CSO | 0.94 | 2.13 | >100.00 |
| | | LSO-FAME | 20.97 | 5.05 | 24.10 |
| | | SBO-FAME | 20.15 | 4.00 | 19.87 |
| | | CSO-FAME | 16.36 | 1.69 | 10.34 |
| $ka_{PA\_org}$ | L/min | LSO | 0.10 | 0.06 | 61.70 |
| | | SBO | 0.01 | 0.00 | 11.26 |
| | | CSO | 0.63 | 0.49 | 77.81 |
| | | LSO-FAME | 8.00 | 0.00 | 0.04 |
| | | SBO-FAME | 19.92 | 0.00 | 0.00 |
| | | CSO-FAME | 0.01 | 0.00 | 9.21 |
| $Coef_1$ | L/mol | LSO | 4.32 | 1.35 | 31.30 |
| | | SBO | 5.75 | 2.87 | 49.85 |
| | | CSO | 0.33 | 0.56 | >100.00 |
| | | LSO-FAME | 9.06 | 78.85 | >100.00 |
| | | SBO-FAME | 10.68 | 3.30 | 30.85 |
| | | CSO-FAME | 22.12 | 13.37 | 60.44 |

[a] Estimated parameters from the same origin were obtained using only the same source of experiments.

[b]$k_{Ep}(T_{ref})$ and $k_{RO}(T_{ref})$ are expressed in L/mol/min.

Table S5 shows the correlation matrix for all models. In the large majority, the correlation values between the estimated parameters in the model are all lower than 0.95, indicating no severe multicollinearity [59]. This suggests that the estimated kinetic constants are independent, which is a positive sign for the stability and interpretability of the model.

### 3.3.5 Model fits for kinetic models of epoxidation of VOs and FAMEs

Fig 9 shows the parity plots for DB (a) and EP (b) of SBO from the kinetic model and Figs S7-S12 show the other parity plots for all models. In general, the model fits the experimental data quite well, as shown by 18 parity plots of the double bond, epoxidation group, and all concentrations ($[Ep]_{org}$, $[DB]_{org}$, $[PA]_{aq}$, $[PPA]_{aq}$, and $[HP]_{aq}$) in the models of 3 VOs and 3 VO-FAMEs.

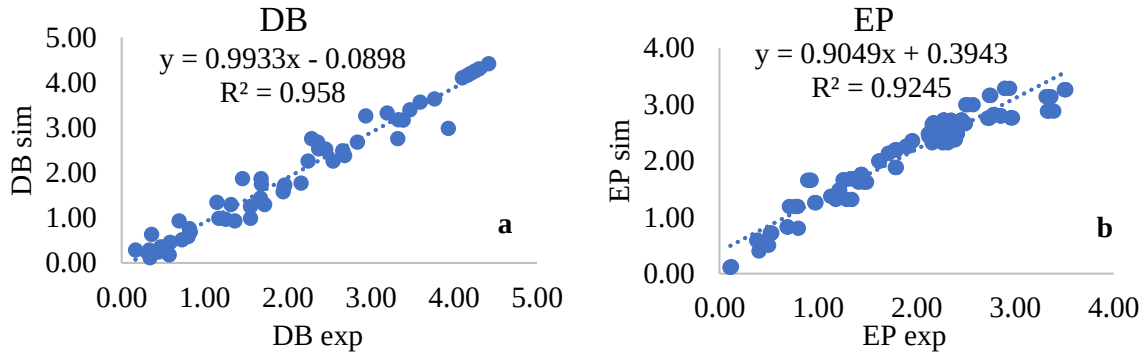


Figure 9 Parity plots for DB (a) and EP (b) of SBO from the kinetic model.

Furthermore, the model fits of the DB and EP in each model are displayed in Fig. 10 (CSO and CSO-FAME), 11 (LSO and LSO-FAME), and 12 (SBO and SBO-FAME). The model slightly tends to overestimate the experimental concentration of DB in SBO, LSO-FAME, and EP in LSO. Generally, it shows great model fits for the models of different organic phases.

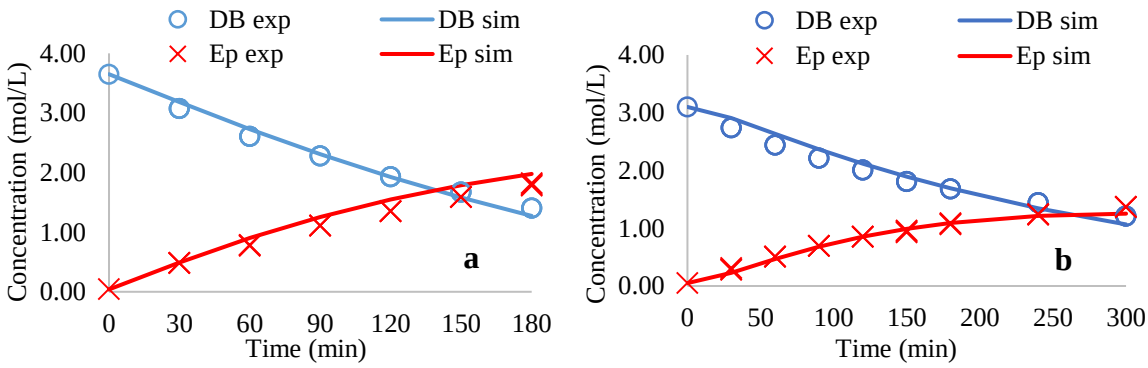


Fig. 10. The fit of models for RUN 3 of CSO (a) and RUN 4 of CSO-FAME (b).

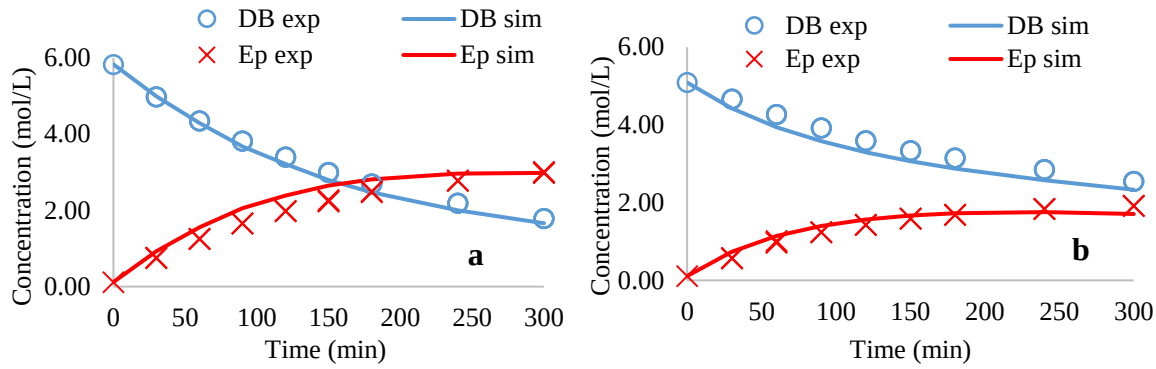


Fig. 11. The fit of models for RUN 2 of LSO (a) and RUN 2 of LSO-FAME (b).

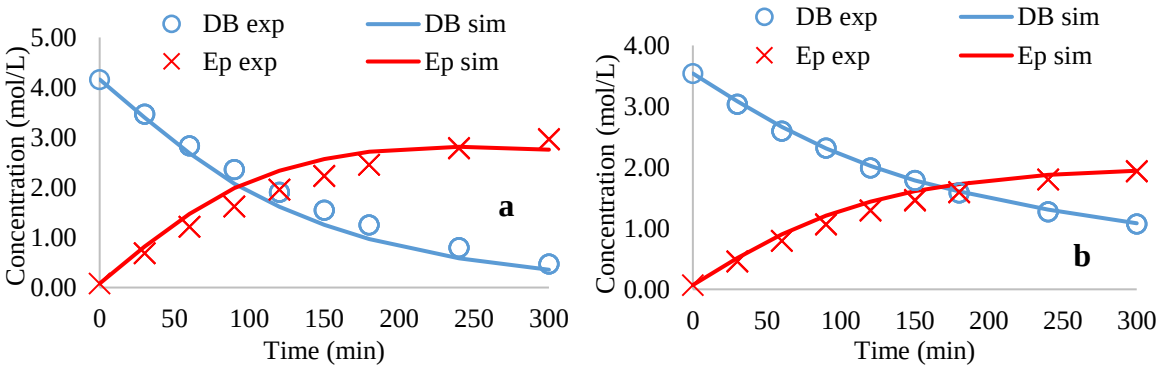


Fig. 12. The fit of models for RUN 2 of SBO (a) and RUN 2 of SBO-FAME (b).

## 3.4 Kinetic model comparison

### 3.4.1 Kinetic model comparison of epoxidation and ring-opening

The comparisons of rate constant in the kinetic model for epoxidation and ring-opening on the double bond concentrations are displayed in Figs 13 (VO) and 14 (VO-FAME). One can notice that rate constants for the epoxidation stage are sensitive to the nature of VO or VO-FAME, whereas this sensitivity is less pronounced for the ring-opening rate constants.

Fig. 13a shows that rate constants for epoxidation evolve in the following order: CSO>SBO>LSO. Besides, one can notice a linear relationship between initial DB concentration and Ln $k_{ep}$ at any temperature, and the rate constant decreases when the initial DB concentration increases. Fig. 13b shows that the rate constant of ring-opening depends less on the initial concentration, and there is a slight increase when the initial concentration increases. Concerning the ring-opening (Fig. 13b), the credible intervals of the estimated activation energy are high for SBO and CSO (Table 1), making it difficult to conclude the linearity of the rate constant of ring-opening.

Fig. 14a shows the same trend for the epoxidation of VO-FAME than for VO. The linearity between the rate constant and initial DB concentration is stronger for VO-FAME than for VO. Fig. 14b shows that the natural logarithm of the ring-opening rate constant does not depend on the initial concentration of DB. The temperature independence of ring-opening reaction towards the nature of VO-FAME and DB concentration could be linked to the fact ring-opening leads to the oligomerization.

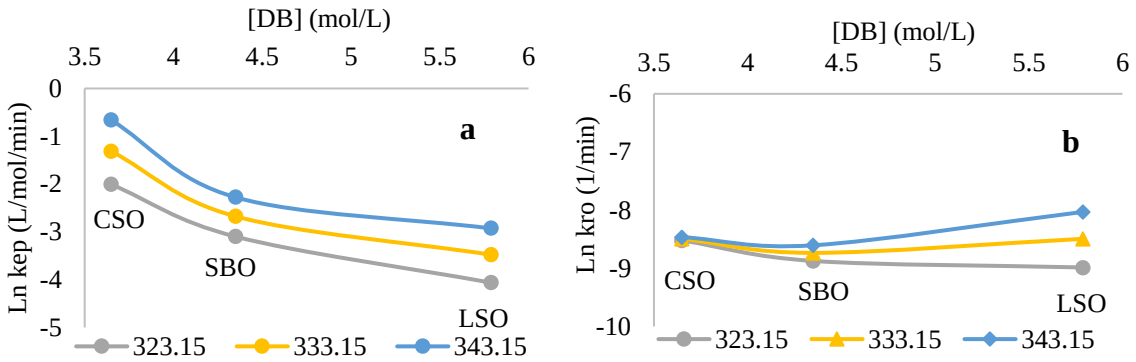


Fig. 13. Kinetic comparison of Ln $k_{ep}$ and Ln $k_{ro}$ versus the initial double bond concentration for the epoxidation of vegetable oils at different temperatures. (Ln $k_{ep}$: The natural logarithm of rate constants for epoxidation; Ln $k_{ro}$: The natural logarithm of rate constants for ring-opening)

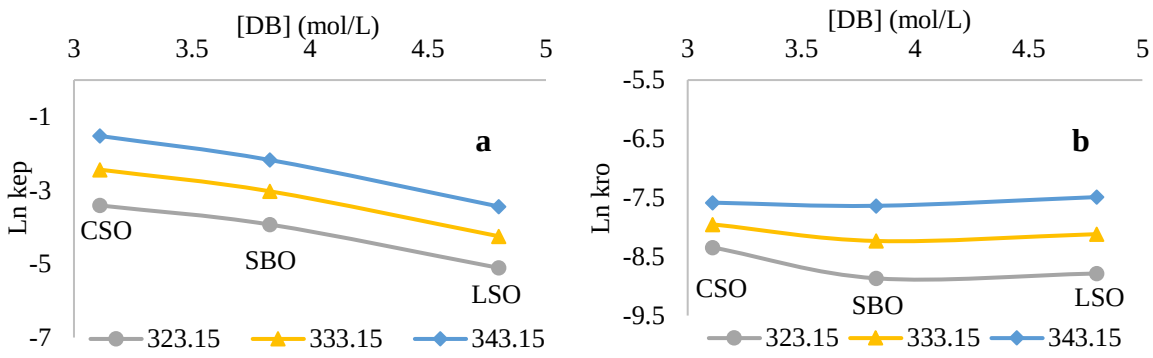


Fig. 14. Kinetic comparison of Ln $k_{ep}$ and Ln $k_{ro}$ versus the initial double bond concentration for the epoxidation of vegetable oil fatty acid methyl esters (VO-FAME) at different temperatures. (Ln $k_{ep}$: The natural logarithm of rate constants for epoxidation; Ln $k_{ro}$: The natural logarithm of rate constants for ring-opening)

# 4 Conclusion

The Prileschajew method is still the most used production method for epoxidized vegetable oils, which use percarboxylic acids. Using propionic acid improves the problem of thermal instability because the heat released by epoxidation is lower compared to formic acid; perpropionic acid is more stable than performic acid, allowing higher recirculation of propionic acid between aqueous and organic phases; and propionic acid is weaker acid compared to formic acid decreasing the side reactions of ring-opening. The use of Amberlite IR-120 aids in catalyzing the perhydrolysis reaction without favoring the ring-opening reaction.

A systematic comparison was made between the epoxidation of CSO, SBO, and LSO and their corresponding FAMEs. An in-depth analysis (density, viscosity, NMR, SEC, FTIR, titration) was carried out to understand the epoxidation and transesterification in different oils. The fatty methyl ester and oxirane ring signals were well identified. Furthermore, CSO shows a faster kinetic in epoxidation than SBO and LSO, CSO-FAME and SBO-FAME show a similar kinetic in epoxidation (faster than LSO).

Kinetic models of CSO, SBO, LSO, and their corresponding FAMEs were developed considering the perhydrolysis of propionic acid, epoxidation of the double bond, and ring-opening of the oxirane ring. The model fits quite well with the experimental concentrations.

An overall comparison of rate constants in different kinetic models for epoxidation and ring-opening was done. The rate constants for epoxidation evolve in the following order: CSO>SBO>LSO. The linearity between the rate constant and initial DB concentration is stronger for VO-FAME than for VO.

A continuation of this work could be the comparison with more different vegetable oils, and developing the kinetic models for fatty acids such as oleic and linoleic acids by using the Prileschajew method via the in situ production of perpropionic acid.

## CRediT authorship contribution statement

**Yudong MENG:** Writing – original draft, Investigation, Visualization, Validation, Software, Methodology, Data curation. **Elano Nery Ferreira:** Writing – review & editing**,** Investigation, Formal Analysis, Data curation. **Nágila Maria Pontes Silva Ricardo**: Writing – review & editing, Project administration, Conceptualization, **Nasreddine Kebir:** Writing – review & editing, Writing – original draft, Supervision, Conceptualization. **Sebastien Leveneur:** Writing – review & editing, Writing – original draft, Supervision, Conceptualization, Project administration.

## Conflicts of Interest

*The authors declare no conflict of interest.*

## Supporting Information

Tables S1-S5 for the density (S1), dynamic viscosity (S2), kinematic viscosity (S3), conversion and selectivity for all runs (S4), and correlation matrix for all models (S5).

Figures S1-S12 for FITR spectra for all compounds (S1-S2), $^{1}$H NMR spectra for all compounds (S3-S4), FITR spectra for all compounds (S5-S6), and parity plots for all kinetic models (S4-S12). This information is available free of charge via the Internet at http://pubs.acs.org/.

## Acknowledgments

This article is part of the ARBRE project. ARBRE is co-funded by the European Union through the European Regional Development Fund (ERDF, agreement n° 00130305) and by Normandy Region (agreement n° 21E05304), via the support of "pôle CTM (Continuum Terre-Mer) and EP2M (Energies, Propulsion, Matière, Matériaux) de Normandie université". The China Scholarship Council: Cooperation Program with the UTs and INSAs (France) is thanked by the authors. We also thank FUNCAP, for the FUNCAP/INSA Rouen Normandie International Cooperation project, Call 02/2022, process SPU 10592660/2022 for the financial support to Elano Nery Ferreira.

## Data availability

Data will be made available on request.

## References


(1) Jagadeesan, D.; Joshi, B.; Parameswaran, P. Chemical Utilisation of CO2 : A Challenge for the Sustainable World. *Resonance* **2015**, *20* (2), 165–176. https://doi.org/10.1007/s12045-015-0163-x.

(2) Adamiec, J.; Kamiński, W.; Markowski, A. S.; Strumiłło, C. Drying of Biotechnological Products. In *Handbook of Industrial Drying, Fourth Edition*; CRC Press, 2014; pp 895–916. https://doi.org/10.1201/b17208.

(3) Galembeck, F.; Abreu Filho, P. P. Perspectives for Biomass Production and Use in Brazil. *Revista Virtual de Quimica*. 2017, pp 274–293. https://doi.org/10.21577/1984-6835.20170018.

(4) Jung, S.; Kim, M.; Lin, K. Y. A.; Park, Y. K.; Kwon, E. E. Biodiesel Synthesis from Bio-Heavy Oil through Thermally Induced Transesterification. *J. Clean. Prod.* **2021**, *294*, 126347. https://doi.org/10.1016/j.jclepro.2021.126347.

(5) Elgharbawy, A. S.; Sadik, W. A.; Sadek, O. M.; Kasaby, M. A.; Elgharbawy, A. S.; Sadik, W. A.; Sadek, O. M.; Kasaby, M. A. A REVIEW ON BIODIESEL FEEDSTOCKS AND PRODUCTION TECHNOLOGIES. *J. Chil. Chem. Soc.* **2021**, *66* (1), 5098–5109. https://doi.org/10.4067/S0717-97072021000105098.

(6) Win, S. S.; Trabold, T. A. Sustainable Waste-to-Energy Technologies: Transesterification. *Sustain. Food Waste-to-Energy Syst.* **2018**, 89–109. https://doi.org/10.1016/B978-0-12-811157-4.00006-1.

(7) Directorate-General for Energy. *Bioenergy report outlines progress being made across the EU*. European Commission. https://energy.ec.europa.eu/news/bioenergy-report-outlines-progress-being-made-across-eu-2023-10-27_en#:~:text=Final consumption of biofuels in,consumption in the transport sector.

(8) Gaglieri, C.; Alarcon, R. T.; de Moura, A.; Bannach, G. Vegetable Oils as Monomeric and Polymeric Materials: A Graphical Review. *Curr. Res. Green Sustain. Chem.* **2022**, *5*, 100343. https://doi.org/10.1016/j.crgsc.2022.100343.

(9) Fernández-Silva, S. D.; Delgado, M. A.; Ruiz-Méndez, M. V.; Giráldez, I.; García-Morales, M. Potential Valorization of Waste Cooking Oils into Sustainable Bio-Lubricants. *Ind. Crops Prod.* **2022**, *185*, 115109. https://doi.org/10.1016/j.indcrop.2022.115109.

(10) Molnár-Kiss, A. V.; Nagy, R. Investigation of Some Food Industrial Vegetable Oil-Based Nonionic Surfactants. *Waste and Biomass Valorization* **2024**, *15* (2), 917–921. https://doi.org/10.1007/s12649-023-02200-w.

(11) Meng, Y.; Taddeo, F.; Aguilera, A. F.; Cai, X.; Russo, V.; Tolvanen, P.; Leveneur, S. The Lord of the Chemical Rings: Catalytic Synthesis of Important Industrial Epoxide Compounds. *Catalysts*. MDPI July 1, 2021. https://doi.org/10.3390/catal11070765.

(12) Cai, X.; Zheng, J. L.; Wärnå, J.; Salmi, T.; Taouk, B.; Leveneur, S. Influence of Gas-Liquid Mass Transfer on Kinetic Modeling: Carbonation of Epoxidized Vegetable Oils. *Chem. Eng. J.* **2017**, *313*, 1168–1183. https://doi.org/10.1016/j.cej.2016.11.012.

(13) Pérez-Sena, W. Y.; Cai, X.; Kebir, N.; Vernières-Hassimi, L.; Serra, C.; Salmi, T.; Leveneur, S. Aminolysis of Cyclic-Carbonate Vegetable Oils as a Non-Isocyanate Route for the Synthesis of Polyurethane: A Kinetic and Thermal Study. *Chem. Eng. J.* **2018**, *346*, 271–280. https://doi.org/10.1016/J.CEJ.2018.04.028.

(14) Rayung, M.; Ghani, N. A.; Hasanudin, N. A Review on Vegetable Oil-Based Non Isocyanate Polyurethane: Towards a Greener and Sustainable Production Route. *RSC Advances*. The Royal Society of Chemistry March 2024, pp 9273–9299. https://doi.org/10.1039/d3ra08684d.

(15) Carré, C.; Ecochard, Y.; Caillol, S.; Avérous, L. From the Synthesis of Biobased Cyclic Carbonate to Polyhydroxyurethanes: A Promising Route towards Renewable Non-Isocyanate Polyurethanes. *ChemSusChem*. John Wiley & Sons, Ltd August 2019, pp 3410–3430. https://doi.org/10.1002/cssc.201900737.

(16) Danov, S. M.; Kazantsev, O. A.; Esipovich, A. L.; Belousov, A. S.; Rogozhin, A. E.; Kanakov, E. A. Recent Advances in the Field of Selective Epoxidation of Vegetable Oils and Their Derivatives: A Review and Perspective. *Catalysis Science and Technology*. The Royal Society of Chemistry August 2017, pp 3659–3675. https://doi.org/10.1039/c7cy00988g.

(17) Wisniak, J.; Cancino, A.; Vega, J. C. Epoxidation of Anchovy Oils. A Study of Variables. *I&EC Prod. Res. Dev.* **1964**, *3* (4), 306–311. https://doi.org/10.1021/i360012a012.

(18) Wisniak, J.; Navarrete, E. Epoxidation Of Fish Oil Kinetic and Optimization Model. *Ind. Eng. Chem. Prod. Res. Dev.* **1970**, *9* (1), 33–41. https://doi.org/10.1021/I360033A006.

(19) Marriam, F.; Irshad, A.; Umer, I.; Asghar, M. A.; Atif, M. Vegetable Oils as Bio-Based Precursors for Epoxies. *Sustain. Chem. Pharm.* **2023**, *31*, 100935. https://doi.org/10.1016/J.SCP.2022.100935.

(20) Thomas, J.; Patil, R. Enabling Green Manufacture of Polymer Products via Vegetable Oil Epoxides. *Ind. Eng. Chem. Res.* **2023**, *62* (4), 1725–1735. https://doi.org/10.1021/ACS.IECR.2C03867/ASSET/IMAGES/MEDIUM/IE2C03867_0003.GIF.

(21) Scotti, N.; Ravasio, N.; Psaro, R.; Evangelisti, C.; Dworakowska, S.; Bogdal, D.; Zaccheria, F. Copper Mediated Epoxidation of High Oleic Natural Oils with a Cumene-O2 System. *Catal. Commun.* **2015**, *64*, 80–85. https://doi.org/10.1016/J.CATCOM.2015.02.008.

(22) Perez-Sena, W. Y.; Wärnå, J.; Eränen, K.; Tolvanen, P.; Estel, L.; Leveneur, S.; Salmi, T. Use of Semibatch Reactor Technology for the Investigation of Reaction Mechanism and Kinetics: Heterogeneously Catalyzed Epoxidation of Fatty Acid Esters. *Chem. Eng. Sci.* **2021**, *230*. https://doi.org/10.1016/J.CES.2020.116206.

(23) Bonon, A. J.; Kozlov, Y. N.; Bahú, J. O.; Filho, R. M.; Mandelli, D.; Shul'pin, G. B. Limonene Epoxidation with H2O2 Promoted by Al2O3: Kinetic Study, Experimental Design. *J. Catal.* **2014**, *319*, 71–86. https://doi.org/10.1016/J.JCAT.2014.08.004.

(24) Dworakowska, S.; Tiozzo, C.; Niemczyk-Wrzeszcz, M.; Michorczyk, P.; Ravasio, N.; Psaro, R.; Bogdał, D.; Guidotti, M. Mesoporous Molecular Sieves Containing Niobium(V) as Catalysts for the Epoxidation of Fatty Acid Methyl Esters and Rapeseed Oil. *J. Clean. Prod.* **2017**, *166*, 901–909. https://doi.org/10.1016/J.JCLEPRO.2017.08.098.

(25) Maiti, S. K.; Snavely, W. K.; Venkitasubramanian, P.; Hagberg, E. C.; Busch, D. H.; Subramaniam, B. Reaction Engineering Studies of the Epoxidation of Fatty Acid Methyl Esters with Venturello Complex. *Ind. Eng. Chem. Res.* **2019**, *58* (7), 2514–2523. https://doi.org/10.1021/acs.iecr.8b05977.

(26) Zheng, J. L.; Wärnå, J.; Salmi, T.; Burel, F.; Taouk, B.; Leveneur, S. Kinetic Modeling Strategy for an Exothermic Multiphase Reactor System: Application to Vegetable Oils Epoxidation Using Prileschajew Method. *AIChE J.* **2016**, *62* (3), 726–741. https://doi.org/10.1002/AIC.15037.

(27) Bai, Y.; Wang, J.; Liu, D.; Zhao, X. Conversion of Fatty Acid Methyl Ester to Epoxy Plasticizer by Auto-Catalyzed in Situ Formation of Performic Acid: Kinetic Modeling and Application of the Model. *J. Clean. Prod.* **2020**, *259*, 120791. https://doi.org/10.1016/j.jclepro.2020.120791.

(28) de Haro, J. C.; Izarra, I.; Rodríguez, J. F.; Pérez, Á.; Carmona, M. Modelling the Epoxidation Reaction of Grape Seed Oil by Peracetic Acid. *J. Clean. Prod.* **2016**, *138*, 70–76. https://doi.org/10.1016/J.JCLEPRO.2016.05.015.

(29) Turco, R.; Tesser, R.; Russo, V.; Cogliano, T.; Di Serio, M.; Santacesaria, E. Epoxidation of Linseed Oil by Performic Acid Produced in Situ. *Ind. Eng. Chem. Res.* **2021**, *60* (46), 16607–16618. https://doi.org/10.1021/ACS.IECR.1C02212/ASSET/IMAGES/LARGE/IE1C02212_0014.JPEG.

(30) Maia, D. L. H.; Fernandes, F. A. N. Influence of Carboxylic Acid in the Production of Epoxidized Soybean Oil by Conventional and Ultrasound-Assisted Methods. *Biomass Convers. Biorefinery* **2022**, *12* (12), 5861–5868. https://doi.org/10.1007/S13399-020-01130-0/METRICS.

(31) Leveneur, S. Thermal Safety Assessment through the Concept of Structure-Reactivity: Application to Vegetable Oil Valorization. *Org. Process Res. Dev.* **2017**, *21* (4), 543–550. https://doi.org/10.1021/ACS.OPRD.6B00405.

(32) Karadeniz, K.; Aki, H.; Sen, M. Y.; Çaliko₰lu, Y. Ring Opening of Epoxidized Soybean Oil with Compounds Containing Two Different Functional Groups. *JAOCS, J. Am. Oil Chem. Soc.* **2015**, *92* (5), 725–731. https://doi.org/10.1007/s11746-015-2638-z.

(33) Campanella, A.; Baltanás, M. A. Degradation of the Oxirane Ring of Epoxidized Vegetable Oils in Liquid–Liquid Heterogeneous Reaction Systems. *Chem. Eng. J.* **2006**, *118* (3), 141–152. https://doi.org/10.1016/J.CEJ.2006.01.010.

(34) Meng, Y.; Kebir, N.; Leveneur, S. Reactivity and Structure: Epoxidation of Cottonseed Oil and the Corresponding Fatty Acid Methyl Ester. *Biomass Convers. Biorefinery* **2023**, 1–12. https://doi.org/10.1007/S13399-023-04985-1/METRICS.

(35) Campanella, A.; Baltanás, M. A. Degradation of the Oxirane Ring of Epoxidized Vegetable Oils with Solvated Acetic Acid Using Cation-Exchange Resins. *Eur. J. Lipid Sci. Technol.* **2004**, *106* (8), 524–530. https://doi.org/10.1002/EJLT.200400965.

(36) Cai, X.; Ait Aissa, K.; Estel, L.; Leveneur, S. Investigation of the Physicochemical Properties for Vegetable Oils and Their Epoxidized and Carbonated Derivatives. *J. Chem. Eng. Data* **2018**, *63* (5), 1524–1533. https://doi.org/10.1021/ACS.JCED.7B01075.

(37) Campanella, A.; Fontanini, C.; Baltanás, M. A. High Yield Epoxidation of Fatty Acid Methyl Esters with Performic Acid Generated in Situ. *Chem. Eng. J.* **2008**, *144* (3), 466–475. https://doi.org/10.1016/J.CEJ.2008.07.016.

(38) Siudem, P.; Zielińska, A.; Paradowska, K. Application of 1H NMR in the Study of Fatty Acids Composition of Vegetable Oils. *J. Pharm. Biomed. Anal.* **2022**, *212*, 114658. https://doi.org/10.1016/J.JPBA.2022.114658.

(39) Paquot, C. 2.504. Determination of Thep-Anisidine Value (p-A.V.). *Stand. Methods Anal. Oils, Fats Deriv.* **2013**, 143–144.

(40) Maerker, G. Determination of Oxirane Content of Derivatives of Fats. *J. Am. Oil Chem. Soc.* **1965**, *42* (4), 329–332. https://doi.org/10.1007/BF02540140.

(41) Greenspan, F. P.; MacKellah, D. G. Analysis of Aliphatic Per Acids. *Anal. Chem.* **1948**, *20* (11), 1061–1063. https://doi.org/10.1021/AC60023A020.

(42) Cai, X.; Zheng, J. L.; Aguilera, A. F.; Vernières-Hassimi, L.; Tolvanen, P.; Salmi, T.; Leveneur, S. Influence of Ring-Opening Reactions on the Kinetics of Cottonseed Oil Epoxidation. *Int. J. Chem. Kinet.* **2018**, *50* (10), 726–741. https://doi.org/10.1002/KIN.21208.

(43) Knothe, G.; Steidley, K. R. A Comprehensive Evaluation of the Density of Neat Fatty Acids and Esters. *J. Am. Oil Chem. Soc.* **2014**, *91* (10), 1711–1722. https://doi.org/10.1007/S11746-014-2519-X.

(44) Pratas, M. J.; Freitas, S.; Oliveira, M. B.; Monteiro, S. C.; Lima, A. S.; Coutinho, J. A. P. Densities and Viscosities of Fatty Acid Methyl and Ethyl Esters. *J. Chem. Eng. Data* **2010**, *55* (9), 3983–3990. https://doi.org/10.1021/JE100042C/ASSET/IMAGES/JE-2010-00042C_M003.GIF.

(45) Rabelo, S. N.; Ferraz, V. P.; Oliveira, L. S.; Franca, A. S. FTIR Analysis for Quantification of Fatty Acid Methyl Esters in Biodiesel Produced by Microwave-Assisted Transesterification. *Int. J. Environ. Sci. Dev.* **2015**, *6* (12), 964–969. https://doi.org/10.7763/IJESD.2015.V6.730.

(46) Tavassoli-Kafrani, M. H.; van de Voort, F. R.; Curtis, J. M. The Use of ATR-FTIR Spectroscopy to Measure Changes in the Oxirane Content and Iodine Value of Vegetable Oils during

Epoxidation. *Eur. J. Lipid Sci. Technol.* **2017**, *119* (7), 1600354. https://doi.org/10.1002/ejlt.201600354.

(47) Wai, P. T.; Jiang, P.; Shen, Y.; Zhang, P.; Gu, Q.; Leng, Y. Catalytic Developments in the Epoxidation of Vegetable Oils and the Analysis Methods of Epoxidized Products. *RSC Advances*. Royal Society of Chemistry 2019, pp 38119–38136. https://doi.org/10.1039/c9ra05943a.

(48) Esen, H.; Çayli, G. Epoxidation and Polymerization of Acrylated Castor Oil. *Eur. J. Lipid Sci. Technol.* **2016**, *118* (6), 959–966. https://doi.org/10.1002/EJLT.201500132.

(49) Sienkiewicz, A. M.; Czub, P. The Unique Activity of Catalyst in the Epoxidation of Soybean Oil and Following Reaction of Epoxidized Product with Bisphenol A. *Ind. Crops Prod.* **2016**, *83*, 755–773. https://doi.org/10.1016/J.INDCROP.2015.11.071.

(50) Meng, Y.; Kebir, N.; Cai, X.; Leveneur, S. In-Depth Kinetic Modeling and Chemical Analysis for the Epoxidation of Vegetable Oils in a Liquid–Liquid–Solid System. *Catalysts* **2023**, *13* (2), 274. https://doi.org/10.3390/catal13020274.

(51) Leveneur, S.; Zheng, J.; Taouk, B.; Burel, F.; Wärnå, J.; Salmi, T. Interaction of Thermal and Kinetic Parameters for a Liquid-Liquid Reaction System: Application to Vegetable Oils Epoxidation by Peroxycarboxylic Acid. *J. Taiwan Inst. Chem. Eng.* **2014**, *45* (4), 1449–1458. https://doi.org/10.1016/J.JTICE.2014.01.015.

(52) Musante, R. L.; Grau, R. J.; Baltanás, M. A. Kinetic of Liquid-Phase Reactions Catalyzed by Acidic Resins: The Formation of Peracetic Acid for Vegetable Oil Epoxidation. *Appl. Catal. A Gen.* **2000**, *197* (1), 165–173. https://doi.org/10.1016/S0926-860X(99)00547-5.

(53) Stewart, W. E.; Caracotsios, M. Computer-Aided Modeling of Reactive Systems. *Comput. Model. React. Syst.* **2007**, 1–267. https://doi.org/10.1002/9780470282038.

(54) Caracotsios, M.; Stewart, W. E. Sensitivity Analysis of Initial Value Problems with Mixed Odes and Algebraic Equations. *Comput. Chem. Eng.* **1985**, *9* (4), 359–365. https://doi.org/10.1016/0098-1354(85)85014-6.

(55) Stewart, W. E.; Caracotsios, M.; Sørensen, J. P. Parameter Estimation from Multiresponse Data. *AIChE J.* **1992**, *38* (5), 641–650. https://doi.org/10.1002/AIC.690380502.

(56) van Boekel, M. A. J. S. On the Pros and Cons of Bayesian Kinetic Modeling in Food Science. *Trends Food Sci. Technol.* **2020**, *99*, 181–193. https://doi.org/10.1016/j.tifs.2020.02.027.

(57) Buzzi-Ferraris, G. Planning of Experiments and Kinetic Analysis. *Catal. Today* **1999**, *52* (2–3), 125–132. https://doi.org/10.1016/S0920-5861(99)00070-X.

(58) Prileschajew, N. Oxydation Ungesättigter Verbindungen Mittels Organischer Superoxyde. *Berichte der Dtsch. Chem. Gesellschaft* **1909**, *42* (4), 4811–4815. https://doi.org/10.1002/CBER.190904204100.

(59) Toch, K.; Thybaut, J. W.; Marin, G. B. A Systematic Methodology for Kinetic Modeling of Chemical Reactions Applied to N-Hexane Hydroisomerization. *AIChE J.* **2015**, *61* (3), 880–892. https://doi.org/10.1002/AIC.14680.

# Graphic abstract